PNAS
www.pnas.org

Supplementary Information for

Optimal ligand discrimination by asymmetric dimerization and turnover of interferon receptors

Patrick Binder, Nikolas D. Schnellbächer, Thomas Höfer, Nils B. Becker and Ulrich S. Schwarz

This PDF file includes:

Supporting Information Text

1. Information theoretic framework for ligand discrimination

A. Decomposing ligand discrimination power according to ligand presence and type. The performance for sensing of ligand presence and type is measured by the mutual information

$$I = I[p(x,n)] = \left\langle \log_2 \frac{p(n|x)}{\sum_x p(n|x)p(x)} \right\rangle, \quad [1]$$

as stated in the main text. In the following we derive a decomposition of the information I into partial informations about ligand presence and ligand type, respectively.

We begin by recalling a decomposition property for the information entropy $H[p(i)] = -\langle \log_2 p(i) \rangle$, of a finite probability distribution $p(i) \equiv (p(1), \ldots, p(d))$. Namely,

$$H[p(i)] = H[(p(1), 1-p(1))] + (1-p(1))H[p(i|i>1)]. \quad [2]$$

The first term in the decomposition is the entropy of the binary decision $i = 1$ vs. $i > 1$. The second term is the entropy remaining in the case $i > 1$, weighted with its probability. Applied to the variable $x \in \{\alpha, \beta, \varnothing\}$, this relation yields

$$\begin{aligned} H[p(x)] &= H[(p(\varnothing), 1-p(\varnothing))] + (1-p(\varnothing))H[p(x|x \in \{\alpha,\beta\})] \\ &= H[p(\pi)] + p(\pi{=}1)H[p(\tau|\pi{=}1)], \end{aligned} \quad [3]$$

where we have introduced new variables π and τ, indicating ligand presence: $\pi(x) = \delta_{x\alpha} + \delta_{x\beta}$, and ligand type when ligand is present: $\tau(x) = x$ when $\pi(x) = 1$, respectively.

The basic relation

$$I[p(x,n)] = H[p(x)] - \langle H[p(x|n)] \rangle, \quad [4]$$

where the average runs over n, by applying Eq. (3) twice and reordering, then becomes

$$\begin{aligned} I[p(x,n)] &= H[p(\pi)] + p(\pi{=}1)H[p(\tau|\pi{=}1)] - \Big\langle H[p(\pi|n)] + p(\pi{=}1|n)H[p(\tau|n,\pi{=}1)] \Big\rangle \\ &= H[p(\pi)] - \langle H[p(\pi|n)] \rangle + p(\pi{=}1)H[p(\tau|\pi{=}1)] + \langle p(\pi{=}1|n)H[p(\tau|n,\pi{=}1)] \rangle \\ &= I[p(\pi,n)] + p(\pi{=}1)\Big\{ H[p(\tau|\pi{=}1)] - \sum_n p(n|\pi{=}1)H[p(\tau|n,\pi{=}1)] \Big\} \\ &= I[p(\pi,n)] + p(\pi{=}1)I[p(\tau,n|\pi{=}1)]. \end{aligned} \quad [5]$$

We conclude that the ligand discrimination power can be written as a weighted sum of two terms, $I = I_\pi + p_\pi I_\tau$. The presence information $I_\pi = I[p(\pi,n)]$ quantifies the performance of detection of any ligand. The type information $I_\tau = I[p(\tau,n|\pi{=}1)]$ is the performance of ligand type detection when ligand is in fact present; it enters with a weight $p_\pi{=}1/2$ due to our choice of input distribution.

B. Readout molecules are Poisson distributed. In most signal transduction pathways, activated receptor complexes C are read out by phosphorylation of intracellular signaling molecules M. The rate of phosphory-

lation is proportional to the number of activated complexes, which for fixed total receptor number R_0 is proportional to the activated receptor fraction f. Assuming constitutive dephosphorylation, we obtain

$$\mathrm{M} \underset{\omega_u}{\overset{f\omega_p}{\rightleftharpoons}} \mathrm{M}_p, \qquad [6]$$

where R_0 is absorbed in ω_p. The master equation for the probability $p(n;t)$ that n out of N readout molecules are phosphorylated at time t reads

$$\frac{\partial p(n;t)}{\partial t} = f\omega_p(N-n+1)p(n-1;t) + \omega_u(n+1)p(n+1;t) - [\omega_u n + f\omega_p(N-n)]\,p(n;t). \qquad [7]$$

Since we are primarily interested in information transmission at the receptor stage, we neglect possible effects of readout molecule depletion and consider a linear regime where only a small fraction of readout molecules are phosphorylated. This corresponds to the limit $N \to \infty$ of a large reservoir of unphosphorylated readout molecules. Defining an effective phosphorylation rate $\tilde{\omega}_p \equiv \omega_p N$, the reactions read

$$\varnothing \underset{\omega_u}{\overset{f\tilde{\omega}_p}{\rightleftharpoons}} \mathrm{M}_p. \qquad [8]$$

The steady state distribution $p(n)$ of these reactions is well-known to be the Poisson distribution with mean $\bar{n}f$ (1),

$$p(n) = \frac{(\bar{n}f)^n}{n!} e^{-\bar{n}f}. \qquad [9]$$

Here, the readout number $\bar{n} = \tilde{\omega}_p/\omega_u$ is the mean phosphorylated readout molecule number at full activation.

C. Recipe for estimating discrimination power. In this section we give a brief overview on how to estimate the mutual information for generic response modules:

1. Determine the steady-state **activation curves** for a given receptor module:

$$f_x(L), \quad x \in \{\alpha, \beta, \varnothing\}. \qquad [10]$$

   f is a function of the ligand concentration L and in general of several other biophysical parameters such as receptor densities R_i and affinities (see also Sec. 3 and 4).

2. Specify the **ligand concentration distributions** for all inputs x:

$$p(L|x), \quad x \in \{\alpha, \beta, \varnothing\}. \qquad [11]$$

   For a discussion on appropriate choices for the ligand concentration distribution see section 2.

3. Specify a **readout noise** $p(n|f)$. Here, we choose a Poisson distribution

$$p(n|f) = \frac{(\bar{n}f)^n}{n!} e^{-\bar{n}f}. \qquad [12]$$

4. Compute the **input-output relation** by using

$$p(n|x) = \int p(n|f_x(L))p(L|x)dL. \quad [13]$$

5. Specify the **input distribution** $p(x)$. Here, we choose

$$p(x) = \begin{cases} 1/2 & x = \varnothing \\ 1/4 & x = \alpha, \beta \end{cases}. \quad [14]$$

6. Finally, calculate the **mutual information**. Since the input x and the output n are discrete, using Eq. (1) from the main text, the mutual information can estimated according to

$$I[p(x,n)] = \sum_{x,n} p(x)p(n\,|\,x)\,\log\left(\frac{p(n\,|\,x)}{\sum_{x'} p(x')p(n\,|\,x')}\right). \quad [15]$$

2. Physiological cytokine distributions

A. Maximum-entropy distribution. Cytokine receptor systems can be exceptionally sensitive, achieving detection thresholds in the sub-pM range. However, cytokines are released by producing cells in an inflamed tissue and can therefore reach high concentrations in the μM range locally (2, 3). A model for the cytokine concentration distribution encompassing tissue cells in our out of inflammation, should then incorporate a concentration range that is 'broad, ranging from pM to μM'. In particular, without further information, no concentration scale other than these approximate limits should be imposed. This implies that the distribution $p(L)$ should be invariant under rescaling transformations $L \to \alpha L$, except for adjusting the lower and upper bounds of its support, see e.g. (4). The unique such scale-free distribution is

$$p_{\rm sf}(L) = \begin{cases} \frac{1}{\log(L_{\rm hi}/L_{\rm lo})}\frac{1}{L} & L_{\rm lo} < L < L_{\rm hi} \\ 0 & \text{otherwise} \end{cases}. \quad [16]$$

Transformed into the space of the log-concentration $\ell \equiv \log L$, this distribution is constant:

$$p_{\rm sf}(\ell) = \begin{cases} 1/(\ell_{\rm hi} - \ell_{\rm lo}) & \ell_{\rm lo} < \ell < \ell_{\rm hi} \\ 0 & \text{otherwise} \end{cases}. \quad [17]$$

B. Production-diffusion-degradation mechanism. By considering the process of cytokine production, spreading and degradation, we can perform a more thorough estimate of physiological cytokine distributions. Cytokines such as interferon are produced by a small subset of activated producer cells; they then spread effectively diffusively within the tissue until they are degraded, typically by being taken up by receiver cells. On spatial scales much larger than a cell diameter, the spatial concentration profile thus obeys

$$\partial_t L(\vec{x},t) = k_s s(\vec{x}) + D\Delta L(\vec{x},t) - \mu L(\vec{x},t), \quad [18]$$

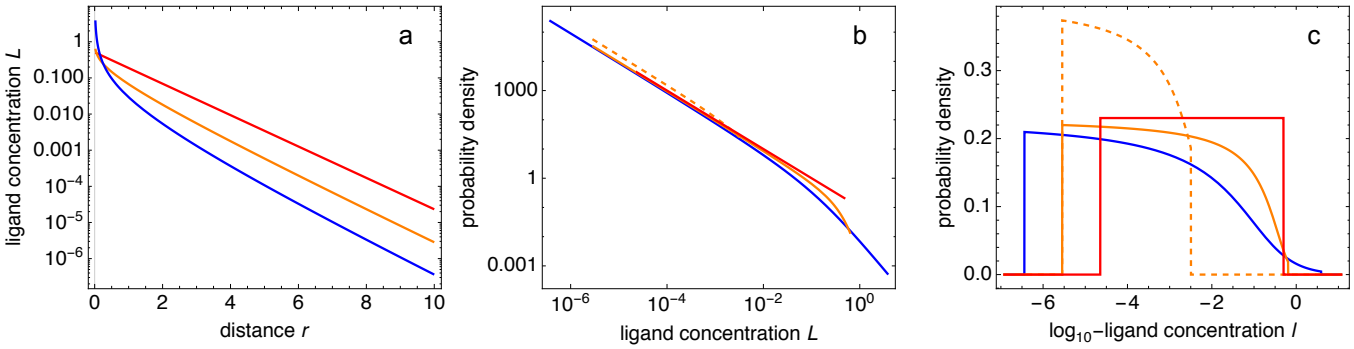

Fig. S1. Ligand profiles $L(r)$ (a) and concentration distributions $p(L)$ in linear and log-concentration space (b and c, respectively). Dimensionalities $d = 1, 2, 3$ are shown in red, orange and blue, respectively. The approximated distribution Eq. (24) outside niches for $d = 2$ is shown dashed; it differs from the numerical exact result mainly due to normalization. Note the good agreement of all distributions with the scale-free $d = 1$ form in the low-concentration regime. Parameter values: $k_s = 1, D = 1, \nu = 1, r_s = 0.02, S = 10$.

where the source term $s(\vec{x}) = \sum_i \delta(\vec{x} - \vec{x}_i)$ is the local density of producer cells at positions $\{x_i\}$, k_s is the cytokine production rate per cell, D is the effective diffusion coefficient, and μ the total degradation rate.

In stationary state, this equation predicts that sparse producing cells are surrounded by niches of elevated cytokine concentration (5) with a characteristic size $\nu = \sqrt{D/\mu}$.

One-dimensional profiles In one spatial dimension (e.g. a columnar tissue) and for a single producing cell at $x_0 = 0$, Eq. (18) has the well-known stationary solution

$$L(x) = \frac{k_s}{2\mu\nu} e^{-\frac{|x|}{\nu}}. \qquad [19]$$

From the spatial profile $L(x)$ we calculate a cytokine distribution $p(L)$ by randomly selecting a tissue cell within a region of size S around the producer and determining the distribution of concentration values the tissue cell is exposed to. That is,

$$p(L) = \int_{-S/2}^{S/2} \frac{1}{S} \delta(L(x) - L)\, dx = \frac{2\nu}{SL}. \qquad [20]$$

This happens to coincide exactly with the scale-free distribution discussed above,

$$p(L) = p_{\mathrm{sf}}(L) \text{ with } L_{\mathrm{hi}} = \frac{k_s}{2\mu\nu} \text{ and } \log \frac{L_{\mathrm{hi}}}{L_{\mathrm{lo}}} = \frac{S}{2\nu}. \qquad [21]$$

In a tissue with multiple producer cells, profiles superimpose, changing the concentration distribution. However, in the relevant limit of sparse producers of density $\rho_s \ll 1/\nu$, we may approximate the cytokine profile by Eq. (19) relative to the nearest producer. Effectively, we are considering individual, well separated niches. Then Eq. (21) still holds when setting the spatial range of integration equal to the spacing of producers, $\sigma \simeq 1/\rho_s$. Of note, the production rate k_s only enters in the support, not the shape of the cytokine distribution.

Two-dimensional profiles In isotropic two-dimensional tissues such as epithelia, cytokines accumulate around producers in circular niches. The radial part of Eq. (18) for a single producer with radius r_s located

in the center of the polar coordinate chart reads, in stationary state,

$$\mu L(r) = D[L'(r)/r + L''(r)];\ \text{with boundary conditions } k_s + 2\pi D r_s L'(r_s) = 0 \text{ and } L(\infty) = 0. \qquad [22]$$

This boundary value problem has a unique solution given in terms of Bessel functions K_i of the second kind,

$$L(r) = L_0 K_0(r/\nu) \ \text{ for } r > r_s, \text{where } L_0 = \frac{k_s}{2\pi D}\frac{1}{(r_s/\nu)K_1(r_s/\nu)} \qquad [23]$$

is a concentration reached roughly at half the niche radius. The maximum concentration at the producer is $L(r_s) \simeq k_s/(2\pi D)\log(2\nu/r_s) \simeq L_0 \log(2\nu/r_s)$ for producers smaller than the niche size. The maximum concentration diverges for decreasing producer size, which shows that the mechanism of production, diffusion and degradation can generate very high local cytokine concentrations in two-dimensional niches. The total amount of ligand in the tissue in stationary state remains at $k_s\nu^2/D = k_s/\mu$.

Outside niches ($r \gg \nu$), to leading order, $L(r) = L_0 e^{-r/\nu}[(r/\nu)^{-1/2} + O(r/\nu)^{-3/2}]$. Within this approximation we can evaluate the concentration distribution for a random tissue cell within a radius S of the producer, as in Eq. (20). We obtain

$$p(L) \simeq \begin{cases} \frac{2}{W(2L_0^2/L(S)^2)-W(2)}\frac{W(2L_0^2/L^2)}{1+W(2L_0^2/L^2)}\frac{1}{L} & L(S) < L < L_0, \\ 0 & \text{otherwise} \end{cases}, \qquad [24]$$

where W denotes the Lambert W function, and we have cut away the small fraction of cells at high concentrations $L > L_0$ within niches. Outside niches ($L \ll L_0$), this distribution is approximated by the limiting form $p(L) \propto L^{-1}$.

Together this shows that when producer cells at density $\rho_s \ll \nu^{-2}$ are sparse in a two-dimensional tissue, the vast majority of non-niche tissue cells is subject to a concentration distribution that is again well approximated by the scale-free distribution: $p(L) \simeq p_{\text{sf}}$ with $L_{\text{lo}} \simeq L(\rho_s^{-1/2})$ and $L_{\text{hi}} \simeq L_0 \simeq k_s/(2\pi D)$. Only for the highest concentrations, we expect corrections that lead to some density extending up to $L(r_s)$.

Three-dimensional profiles We repeat the calculation for three-dimensional tissues with spherical niches. The radial part of Eq. (18) now reads

$$\mu L(r) = D[2L'(r)/r + L''(r)];\ \text{with boundary conditions } k_s + 4\pi D r_s^2 L'(r_s) = 0 \text{ and } L(\infty) = 0. \qquad [25]$$

The solution is

$$L(r) = L_0\frac{e^{-r/\nu}}{r/\nu} \ \text{ for } r > r_s, \text{where } L_0 = \frac{k_s}{4\pi D\nu}\frac{1}{(r_s/\nu+1)e^{-r_s/\nu}}. \qquad [26]$$

Again, L_0 is attained at around half the niche radius, and the total amount of ligand evaluates to k/μ. The maximal concentration is $L(r_s) = L_0\frac{e^{-r_s/\nu}}{r_s/\nu} = \frac{k_s}{4\pi D\nu}\frac{1}{r_s/\nu+(r_s/\nu)^2}$. For decreasing producer size, $L_0 \to k_s/(4\pi D\nu)$ and, as in two dimensions, $L(r_s)$ diverges, indicating that high local concentrations are possible around producing cells.

The comparatively simpler form of the ligand profile here allows us to evaluate the concentration

distribution exactly. The result is similar to the two-dimensional case:

$$p(L) = \begin{cases} \frac{\nu}{S-r_s} \frac{W(L_0/L)}{1+W(L_0/L)} \frac{1}{L} & L(S) < L < L(r_s), \\ 0 & \text{otherwise} \end{cases}. \quad [27]$$

As before, the factor involving the W functions tends towards 1 away from the niches where $L \ll L_0$. Thus, when producer cells are sparse at density $\rho_s \ll \nu^{-3}$, the concentration distribution is well approximated by the scale-free distribution: $p(L) \simeq p_{\text{sf}}$ with $L_{\text{lo}} \simeq L(\rho_s^{-1/3})$ and $L_{\text{hi}} \simeq L_0 \simeq k_s/(4\pi D\nu)$. Again, some density extends further up to $L(r_s)$.

C. Summary. In one dimension, the production-diffusion-degradation model of cytokine spreading generates exponential ligand profiles with niches of characteristic size ν set by diffusion coefficient and degradation rate exclusively. Assuming sparse producers, this leads to a ligand concentration distribution of scale-free form p_{sf}, Eq. (16).

In $d = 2$ or 3 dimensions, the characteristic niche size remains ν, but within the niche, the ligand profiles get steeper, reaching high concentrations at the producer cells. These only affect a small fraction $\rho_s\nu^d$ of tissue cells. For the vast majority of non-niche cells, the ligand profile shows small corrections to the simple exponential decay, see Fig. S1a. Consequently, most cells experience a nearly scale-free ligand distribution ω_{sf}, which extends up to the niche boundary concentration L_0. Few cells within a niche experience higher concentrations; the distribution tapers off as $L \to L(r_s)$ (Fig. S1bc).

In the main text, we approximate physiological cytokine distributions by the scale-free distribution p_{sf} throughout, since this gives a simple and good approximation for small, sparse producers in any dimension.

3. Equilibrium response curves

In the following we derive expressions for the fraction f of activated receptors as a function of ligand concentration L,

$$f(L) = \frac{C}{C_{\max}}, \quad [28]$$

where $C_{(\max)}$ denotes the (maximal) concentration of activated receptors C. The fractional response f is also called *binding curve*, or equivalently *dose response curve*.

A. Allosteric transmission. As the simplest receptor-ligand model we consider the reversible binding of a ligand L to a single-unit transmembrane receptor R, which yields an active ligand-receptor complex C ≡ RL according to

$$\mathrm{R} + \mathrm{L} \underset{k_u}{\overset{k_b}{\rightleftharpoons}} \mathrm{C}. \quad [29]$$

Here we impose receptor (mass-)conservation, $R(t) + C(t) = R_0 = const.$ The equilibrium concentration of activated receptors then results as

$$C = R_0 \frac{L}{K + L}, \qquad [30]$$

where K is the equilibrium dissociation constant given by

$$K = \frac{R \times L}{C} = \frac{k_u}{k_b}. \qquad [31]$$

Because $C_{\max} = R_0$, Eq. (28) gives the response curve by

$$f(L) = \frac{L}{K + L} \qquad [32]$$

with half saturation (receptor occupancy) at $L = K$. Thus, f corresponds to the standard *Hill curve* with Hill coefficient $n = 1$. By rescaling the ligand concentration L by its dissociation constant K, we obtain a universal binding curve

$$f(L) = \Phi(L/K) \quad \text{with} \quad \Phi(x) \equiv \frac{x}{1 + x}, \qquad [33]$$

onto which all binding curves for different ligand affinities collapse.

B. Ligand-independent binding mode in receptor dimerization. Sensing by dimerization involves two types of ligand-binding reactions: Association of ligand from the bulk solution, $\mathrm{R} + \mathrm{L} \rightleftharpoons \mathrm{RL}$ with dissociation constant K^B and cross-linking within the two-dimensional membrane, $\mathrm{RL} + \mathrm{R} \rightleftharpoons \mathrm{RLR}$ with dissociation constant K^X. In both (forward) reactions, the same new $\mathrm{R} \cdot \mathrm{L}$ non-covalent bond is formed, but the binding free energies are different. We separate the binding free energy into two terms,

$$\Delta G = \Delta G_{\mathrm{bond}} + \Delta G_{\mathrm{struct}}.$$

Here, G_{bond} is the part of the binding free energy that is due to local residue-residue interactions at the ligand-receptor binding interface, such as the formation of hydrogen bonds, salt bridges or local nonpolar interactions. By contrast, G_{struct} is the binding free energy arising on the scale of the entire molecule; it contains a conformational internal energy due to overall structural deformations in the complex and the configurational entropy of the complex partners.

Because configurational entropy loss and overall structural changes are different upon binding from bulk solution compared to cross-linking, the molecular-scale free energy change differs between the two binding reactions: $\Delta\Delta G_{\mathrm{struct}} \equiv \Delta G^B_{\mathrm{struct}} - \Delta G^X_{\mathrm{struct}} \neq 0$.

We now make the plausible simplifying assumption that the binding mode of ligand and receptor remains unchanged under all conditions. That is, residue-residue contacts are the same in the RL complex and at both interfaces of the RLR complex, so that $\Delta\Delta G_{\mathrm{bond}} \equiv \Delta G^B_{\mathrm{bond}} - \Delta G^X_{\mathrm{bond}} = 0$. Furthermore, ligands of different affinities differ in their local residue-residue contacts but not in the overall structure of the RL and RLR complexes. Thus, ΔG_{bond} but not $\Delta G_{\mathrm{struct}}$ depends on ligand type.

Table S1. Binding length scales λ for the IFN recpetor system

IFN	receptor	λ(nm)	ref.
α2 wt	IFNAR1	5.1; 12.2; 4.8; 11.1	(7–10)
	IFNAR2	5.6; 18.6	(7, 9)
α2 YNS	IFNAR1	5.5	(7)
	IFNAR2	4.5	(7)
α2 R144A	IFNAR1	22.0; 8.8	(8, 9)
	IFNAR2	8.7	(9)
α2 M148A	IFNAR1	11.2	(8)
α2 R120E	IFNAR1	< 40.0	(10)

The assumption of an unchanged binding mode implies that the length scale $\lambda = K^X/K^B$ is a ligand-independent constant. This follows by observing that with a constant binding mode, $\Delta\Delta G = \Delta\Delta G_{\text{struct}}$ is independent of the ligand type. Indeed, using the standard thermodynamic relation for bimolecular dissociation constants,

$$K = c^0 e^{\beta\Delta G^0},$$

where β is the inverse thermal energy and the free energy ΔG^0 corresponds to the reference concentration c^0, we find

$$\lambda = \frac{K^X}{K^B} = \frac{c^0_{2d} e^{\beta\Delta G^{X,0}}}{c^0_{3d} e^{\beta\Delta G^{B,0}}} = \frac{c^0_{2d}}{c^0_{3d}} e^{-\beta\Delta\Delta G^0_{\text{struct}}}. \quad [34]$$

We remark that a ligand-independent length scale λ was already invoked in (6) but emphasize that at this stage it is a plausible assumption, not a thermodynamic identity.

Importantly, in the IFNAR system the assumption of a constant binding mode is supported by experimental data. First, the IFN-IFNAR complexes are structurally highly similar (2), which suggests that ligand-dependent changes are local. Second, bulk and crosslinking dissociation constants for a range of IFNα ligands have been measured independently in biochemical experiments; their ratios, Eq. (34) are found in agreement to within the experimental error, see table S1. For this study we use $\lambda = 5$nm.

C. Homodimerization. Next, we look at the binding curve for a homodimerizing receptor system. That is, we consider the reaction scheme

$$\mathrm{R} + \mathrm{L} \underset{k_u}{\overset{2k_b}{\rightleftharpoons}} \mathrm{RL}, \quad [35a]$$

$$\mathrm{RL} + \mathrm{R} \underset{2k_d}{\overset{k_a}{\rightleftharpoons}} \mathrm{C}, \quad [35b]$$

where a bivalent ligand L can cross-link two monovalent receptors R to form a ternary receptor complex $\mathrm{C} \equiv \mathrm{RLR}$. The factor of two in Eq. (35a) occurs because a free receptor R can bind either of the two binding sites from the ligand L and k_b corresponds to one binding site. The occurrence of factor two in Eq. (35b) is due to fact that either bound receptors from C can dissociate. We use $K^B = k_u/k_b$ to denote the equilibrium dissociation constant for the ligand binding reaction from bulk solution, per ligand binding site, and $K^X = k_d/k_a$ for the equilibrium dissociation constant of the receptor cross-linking reaction within

the membrane (X for cross-linking), per binding site. To derive the binding curve we apply the law of mass action in Eq. (35), which yields

$$K^B = \frac{2R \times L}{RL}, \qquad K^X = \frac{R \times RL}{2C}. \tag{36}$$

Combined with receptor mass conservation, $R(t) + RL(t) + 2C(t) = 2R_0 = const.$, this can be written as

$$R^2 + \left(1 + \frac{K^B}{2L}\right) K^X R - \frac{K^B}{L} K^X R_0 = 0. \tag{37}$$

By inserting the positive root of Eq. (37) for R and $RL = (2L/K^B)\, R$, see Eq. (36), in the receptor conservation relation we obtain

$$C = R_0 \left[1 - (\sqrt{\Delta^2 + 2\Delta} - \Delta)\right], \tag{38}$$

where

$$\Delta = \frac{K^X}{R_0} \frac{(2L + K^B)^2}{8LK^B}. \tag{39}$$

To get the response curve f we note that for the homodimerization scheme Eq. (35) the maximal number of activate receptors is $C_{\max} = R_0$. We can then write the fractional binding curve in the following form

$$f(L) = F(\Delta) \equiv 1 - (\sqrt{\Delta^2 + 2\Delta} - \Delta). \tag{40}$$

This result was already obtained by Perelson while studying receptor aggregation by immunoglobulin and is also termed *cross-linking* curve (11).

The cross-linking curve from Eq. (40) attains its maximal activation level $f_{\max}$ for a ligand concentration $L_{\max} = K^B/2$,

$$f_{\max} = F(K^X/R_0). \tag{41}$$

We note that the position of maximal activation depends on K^B, while the maximal activation level $f_{\max}$ is only a function of the ratio R_0/K^X. Since Eq. (39) is symmetric in log space with respect to $L_{\max}$, *i.e.* $\Delta(aL_{\max}) = \Delta(a^{-1}L_{\max})$, the activation curve Eq. (40) is also symmetric.

By applying Eq. (34), *i.e.* assuming $\lambda = K^X/K^B = const.$, the maximal activation level and its position are coupled. Since $df/dK^B < 0$, the response curve Eq. (40) is maximized by vanishing bulk dissociation constant, resulting in an envelope function

$$f_{\text{envelope}}(L) = F(L\lambda/R_0) \tag{42}$$

and a global half-deactivation point

$$L_{\text{deact}} = \frac{R_0}{2\lambda}. \qquad [43]$$

D. Heterodimerization. The heterodimerizing receptor scheme consists of two competing dimerization pathways, which both lead to the formation of an activated receptor complex. Namely, a free ligand can bind first to receptor chain R_1 and then cross-link with R_2, or vice versa. The two independent assembly pathways give rise to the following set of reversible reactions

$$\mathrm{R}_i + \mathrm{L} \underset{k_{u,i}}{\overset{k_{b,i}}{\rightleftharpoons}} \mathrm{R}_i\mathrm{L} \qquad \text{for} \quad i = 1, 2 \qquad [44a]$$

$$\mathrm{R}_i + \mathrm{R}_j\mathrm{L} \underset{k_{d,i}}{\overset{k_{a,i}}{\rightleftharpoons}} \mathrm{C} \qquad \text{for} \quad (i, j) = (1, 2), (2, 1), \qquad [44b]$$

where we use $\mathrm{C} \equiv \mathrm{R}_1\mathrm{L}\mathrm{R}_2 = \mathrm{R}_2\mathrm{L}\mathrm{R}_1$ to denote the active heterodimer complex. Notice, since a receptor R_i can only bind to one specific binding site of the ligand L, Eq. (44) lacks the factors of two as compared to the homodimerizing reaction scheme Eq. (35). At equilibrium the concentrations are governed solely by the four equilibrium dissociation constants

$$K_i^B = \frac{k_{u,i}}{k_{b,i}} \quad \text{and} \quad K_i^X = \frac{k_{d,i}}{k_{a,i}} \qquad i = 1, 2. \qquad [45]$$

However, in equilibrium all reactions must balance individually

$$R_1L = \frac{R_1 \times L}{K_1^B}, \qquad R_2L = \frac{R_2 \times L}{K_2^B}, \qquad [46a]$$

$$\frac{R_2 \times R_1L}{K_2^X} = C = \frac{R_1 \times R_2L}{K_1^X}, \qquad [46b]$$

which shows that the equilibrium constants are constrained by the detailed balance condition

$$K_1^B K_2^X = K_2^B K_1^X. \qquad [47]$$

In Section B, in the context of homodimerization, we introduced a binding length scale λ which relates bulk and membrane ligand-binding constants. The arguments presented there carry through for each of the receptor-binding site pairs. Thus, for each chain R_i individually, λ is independent of ligand binding affinity to R_i. Eq. (47) shows that in addition, λ is the same for R_1 and R_2:

$$\lambda = K_1^X/K_1^B = K_2^X/K_2^B. \qquad [48]$$

To find the equilibrium binding curve we first note two receptor number conservation laws

$$R_i(t) + R_iL(t) + C(t) = R_{i,0} = const. \qquad i = 1, 2. \qquad [49]$$

Combining the conservation laws Eq. (49) with Eq. (46) we find

$$C = \frac{R_T}{2}\left[1 - \left(\sqrt{\tilde{\Delta}^2 + 2\tilde{\Delta} + 1 - \frac{4R_{1,0}R_{2,0}}{R_T^2}} - \tilde{\Delta}\right)\right], \quad [50]$$

where we introduced the total receptor concentration $R_T = R_{1,0} + R_{2,0}$ and defined the dimensionless shortcut

$$\tilde{\Delta} \equiv \frac{K_1^X}{R_T}\frac{(L + K_1^B)(L + K_2^B)}{LK_1^B}. \quad [51]$$

This result was achieved by Perelson studying histamine release by mast cells and basophils (12). Considering 1:1 stoichiometry, *i.e.* $R_{1,0} = R_{2,0} \equiv R_0$, the dose response curve reduces to

$$f(L) = \frac{C}{R_0} = F(\tilde{\Delta}) \quad [52]$$

which corresponds to the binding curve for the homodimerizing system Eq. (40), but with $\tilde{\Delta}$ in place of Δ. Setting both receptor surface concentrations equal changes $\tilde{\Delta}$ to

$$\tilde{\Delta} = \frac{K_1^X}{R_0}\frac{(L + K_1^B)(L + K_2^B)}{2LK_1^B} = \frac{K_2^X}{R_0}\frac{(L + K_1^B)(L + K_2^B)}{2LK_2^B}, \quad [53]$$

where the second identity results from the overall symmetry of the two available assembly pathways. As for the homodimerizing system, it can be shown that Eq. (53), and therefore the activation curve Eq. (52), is symmetric in log space with respect to $L_{\max} = \sqrt{K_1^B K_2^B}$.

Like for the homodimerization, the global length scale λ couples $f_{\max} = F\left(\frac{1}{2}\left[\sqrt{K_1^X/R_0} + \sqrt{K_2^X/R_0}\right]^2\right)$ and $L_{\max}$, resulting in an envelope

$$f_{\text{envelope}}(L) = F\left(\frac{L\lambda}{2R_0}\right) \quad [54]$$

and a global half-deactivation point

$$L_{\text{deact}} = \frac{R_0}{2\lambda}. \quad [55]$$

Here, the envelope is attained for vanishing bulk dissociation constants, since $df/dK_i^B < 0$.

The activation curves for all three equilibrium receptor-ligand binding models are summarized in Table S2. While the single-unit ligand receptor motif is parameterized by a single binding affinity K, the homodimerizing motif is parameterized by K^B, K^X, R_0 and the heterodimerizing by K_1^B, K_2^B, K_2^X and R_0.

E. Symmetric heterodimerization differs from homodimerization. For completeness, we point out a subtle but real difference. A homodimerizing receptor system consists of monovalent receptors R which can bind bivalent ligand at either of the binding sites, see Eq. (35). Thus, free ligand and singly bound ligand-receptor pairs compete for binding to free receptors R. A symmetric heterodimerizing receptor system on the other hand is a motif according to Eq. (44), where two monovalent receptors with structurally different binding

Table S2. Dose response curves f for the three equilibrium receptor-ligand binding motifs

receptor topology	activation curve f	parameters
allosteric	$f = L/(K+L)$	K
homodimerizing	$f = F(\Delta),\ \Delta = \frac{K^X}{R_0}\frac{(2L+K^B)^2}{8LK^B}$	K^B, K^X, R_0
heterodimerizing	$f = F(\tilde{\Delta}),\ \tilde{\Delta} = \frac{K_1^X}{R_0}\frac{(L+K_1^B)(L+K_2^B)}{2LK_1^B}$	K_1^B, K_2^B, K_1^X, R_0

While the allosteric response function follows hyperbolic saturation kinetics (monotonic increase), the two dimerization motifs show a biphasic response, which in log-space has a characteristic bell-shape. $F(\Delta)$ is defined in Eq. (40) and the result for the heterodimeric case assumes $R_{1,0} = R_{2,0} = R_0$ as before.

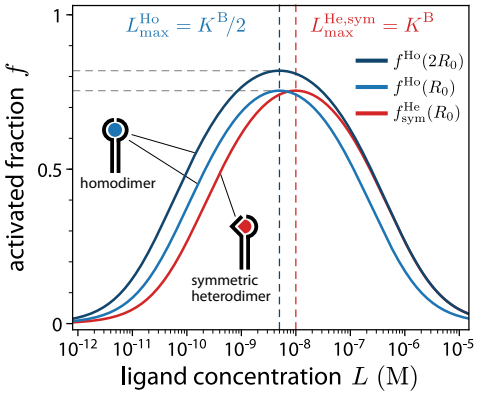

Fig. S2. The activation curve for a homodimer at receptor concentration R_0 (blue) compared to a symmetric heterodimer (red) with the same binding affinities and receptor concentration R_0 for each chain. The shift of the heterodimer curve to higher ligand concentrations is not due to the higher total receptor concentration $R_T = 2R_0$, as the homodimer curve at receptor concentration $2R_0$ (black) shows. Here we used $K^B = 10\mathrm{nM}$, $K^X = 0.2\mu\mathrm{m}^{-2}$ and $R_0 = 10\mu\mathrm{m}^{-2}$.

sites, each cognate to one binding site on the ligand, happen to have identical binding kinetics, *i.e.* $K_1^B = K_2^B$ and $K_1^X = K_2^X$. Hence, $\mathrm{R_1L}$ complexes compete only for free $\mathrm{R_2}$ chains and not for $\mathrm{R_1}$, and vice versa. Concretely, comparing Eq. (53) where $K_1^B = K_2^B$ with the homodimer Eq. (39), the expressions indeed differ. As a result, the activation curves also differ between these two cases if all microscopic rates and R_0 are kept the same, see Fig. S2. In order to obtain a symmetric heterodimerizing system with an activation curve that reproduces the homodimerizing curve exactly, one would have to choose $K_i^B = K^B/2$, keeping $R_0/K_i^X = R_0/K^X$ the same.

4. Steady-state response curves including receptor turnover

To understand the effect of receptor turnover, we revisit the ligand-receptor systems discussed in Sec. 3, but now consider the non-equilibrium steady state resulting from receptor turnover. Out of equilibrium, the activation curves are no longer fully specified by the equilibrium dissociation constants, but instead depend on the full set of rates, roughly doubling the number of parameters, see table S3. For allosteric and homodimerizing systems, we provide closed form expressions for the binding curves. In the heterodimerizing case, binding curves are obtained numerically.

Since there is no evidence for targeted degradation in the IFNAR system, we assume that any membrane bound species ($\mathrm{R}, \mathrm{RL}, \mathrm{C}$) is internalized and degraded with a common degradation rate μ. A constant mean

total receptor number is ensured by reintegration of free receptors R, at rate α:

$$\mathrm{R} \underset{\alpha}{\overset{\mu}{\rightleftharpoons}} \varnothing, \quad \mathrm{RL} \xrightarrow{\mu} \varnothing, \quad \mathrm{C} \xrightarrow{\mu} \varnothing. \tag{56}$$

In steady state, the total surface concentration of a receptor chain is given by the ratio of production and degradation rate, *i.e.*

$$\left.\begin{array}{ll} \text{allosteric:} & R + C \\ \text{homodimerizing:} & \dfrac{R + RL}{2} + C \\ \text{heterodimerizing:} & R_i + R_i L + C \end{array}\right\} = \frac{\alpha}{\mu} \equiv R_0. \tag{57}$$

We set α/μ to equal the receptor concentration R_0, so that the non-equilibrium response curves are consistent with the equilibrium response curves in section 3, in the limit of slow turnover.

A. Turnover shifts allosteric response curves to higher ligand concentration. Combining the reactions Eq. (29) with turnover of receptors Eq. (56), yields a system of ordinary differential equations (ODEs) for the concentrations,

$$\frac{dR}{dt} = -k_b\, R \times L + k_u\, C - \mu\, R + \alpha, \tag{58a}$$

$$\frac{dC}{dt} = k_b\, R \times L - k_u\, C - \mu\, C. \tag{58b}$$

Using Eq. (57), the steady-state fraction of activated receptors is given by

$$f(L) = \Phi\Big(\frac{L}{K + \mu/k_b}\Big), \tag{59}$$

where $K = k_u/k_b$, see Eq. (31), and $\Phi(x)$ is defined in Eq. (33). Comparing with Eq. (32) we see that the shape of the binding curve is unchanged. Turnover merely shifts the curve in log-concentration space, corresponding to a higher effective dissociation $K + \mu/k_b$.

B. Turnover shifts and skews homodimer response curves. Next, we consider the effect of receptor turnover on a homodimerizing receptor system, Eq. (35). Incorporating Eq. (56) results in the ODEs

$$\frac{dR}{dt} = -2k_b\, L \times R + k_u\, RL - k_a\, R \times RL + 2k_d\, C - \mu\, R + \alpha, \tag{60a}$$

$$\frac{dRL}{dt} = 2k_b\, L \times R - k_u\, RL - k_a\, R \times RL + 2k_d\, C - \mu\, RL, \tag{60b}$$

$$\frac{dC}{dt} = k_a\, R \times RL - 2k_d\, C - \mu\, C. \tag{60c}$$

Using Eq. (57), some calculation leads to the steady state activation curve

$$f(L) = 1 - (\sqrt{\Delta_1^2 + 2\Delta_2} - \Delta_1) \tag{61}$$

where we introduced

$$\Delta_1 = \Delta_0 + \frac{\tau_u(2L - K^B)}{(2+\tau_u)(4L + \tau_u K^B)}, \tag{62a}$$

$$\Delta_2 = \Delta_0 + \frac{\tau_u^2 K^B}{2(2+\tau_u)(4L + \tau_u K^B)}, \tag{62b}$$

$$\Delta_0 = \frac{K^X(2+\tau_d)}{8R_0} \frac{[K^B(2+\tau_u) + 4L + \tau_u K^B]^2}{K^B(2+\tau_u)(4L + \tau_u K^B)}, \tag{62c}$$

as well as dimensionless binding times $\tau_{u,d}$, namely

$$\tau_{u,d} = \frac{\mu}{k_{u,d}}. \tag{63}$$

For the limit of no turnover, which corresponds here to $\tau_{u,d} \to 0$ the result is in agreement with Eq. (40). Note that the receptor turnover breaks the symmetry of the response curve in log space. The maximal activation

$$f_{\max} = F([1 + \tau_d/2]K^X/R_0) \tag{64}$$

in Eq. (61) is reached at

$$L_{\max} = \frac{K^B}{2}\left[1 + \frac{\tau_u}{2}\left(1 + \sqrt{1 + \frac{4R_0}{K^X(2+\tau_d)}}\right)\right]. \tag{65}$$

Comparing these results with Eq. (41), receptor turnover decreases the maximal activation and shifts it to higher concentrations.

Taking into account that all ligand-receptor share a single binding mode, see Eq. (34), maximizing Eq. (61) with respect to K^B, yield the half-deactivation point

$$L_{\text{deact}} = \frac{R_0}{2\lambda}\frac{2+3\tau_u}{2+\tau_d}. \tag{66}$$

Comparing Eq. (66) with Eq. (43) illustrates that the turnover can shift the global deactivation point to higher (lower) concentrations for $3\tau_u > \tau_d$ ($3\tau_u < \tau_d$). Intuitively, slow τ_u means bulk ligand unbinding is slower relative to turnover, so that in the deactivating regime, excess binary complexes are removed by turnover, helping activation. Counteracting this effect, slow complex dissociation τ_d means some active complexes are removed before reforming. In combination, whether the deactivation point is shifted to higher (lower) concentration is fully determined by the ratio $k_d/k_u < (>)\, 3$.

Table S3. Parameters and steady state activation curves of the allosteric, homodimerizing and heterodimerizing receptor systems including receptor turnover

receptor topology	activation curve f	parameters
allosteric	$f = L/[K(1+\tau_u)+L]$	K, τ_u
homodimerizing	see Eq. (61)	$K^B, K^X, R_0, \tau_u, \tau_d$
heterodimerizing	numerical	K_1^B, K_2^B, K_2^X, R_0 $\tau_{u,1}, \tau_{u,2}, \tau_{d,1}, \tau_{d,2}$

Dimensionless binding times $\tau_{u,d}$ are defined as in Eq. (63). For the heterodimer, subscripts $i = 1, 2$ indicate the receptor chain.

C. Heterodimerization. Incorporating turnover in the heterodimerizing system, Eq. (44), we arrive at

$$\frac{\mathrm{d}R_i}{\mathrm{d}t} = -k_{b,i}\, R_i \times L + k_{u,i}\, R_i L - k_{a,i}\, R_i \times R_j L + k_{d,i}\, C - \mu\, R_i + \alpha, \tag{67a}$$

$$\frac{\mathrm{d}R_i L}{\mathrm{d}t} = k_{b,i}\, R_i \times L - k_{u,i}\, R_i L - k_{a,j}\, R_j \times R_i L + k_{d,j}\, C - \mu\, R_i L, \tag{67b}$$

$$\frac{\mathrm{d}C}{\mathrm{d}t} = k_{a,1}\, R_1 \times R_2 L + k_{a,2}\, R_2 \times R_1 L - (k_{d,1} + k_{d,2})\, C - \mu\, C, \tag{67c}$$

where the pair of indices runs over $(i, j) = (1, 2), (2, 1)$ to account for the symmetry of the two assembly pathways. We have been unable to solve the steady state of Eq. (67) analytically. Therefore, we determine the response curve numerically. The results of steady state activation curves are summarized in Table S3.

5. Optimizing the ligand discrimination power

In the following we give details on the optimization procedure we used to obtain the reults shown in Figs. 3-5 in the main text and Figs. S3-S4. We optimized the discrimination power I with respect to the equilibrium dissociation constants K^B and in non-equilibrium steady state, additionally with respect to the unbinding rates k_u, k_d. We used Dual Annealing (13) as implemented in the function `dual_annealing` in the package Scipy 1.5.0 (14).

The allowed parameter ranges and values of fixed parameters are given in Table S4. They are chosen to reflect the physiological range of the IFN system and basic biophysical constraints, as follows. The range of the dissociation constants $K^B = 1 - 10^7$pM corresponds roughly to the biological range of

Table S4. Fixed parameter values and optimization bounds for optimizing the ligand discrimination power I

parameter	unit	fixed value / optimization range	ref.
K^B	pM	$1 - 10^7$	(15)
k_u	s^{-1}	$10^{-9} - 0.06 K^B/\mathrm{pM}$	(16)
k_d	s^{-1}	$10^{-9} - 2\times 10^{-6} \lambda K^B/(\mathrm{nm\,pM})$	(16)
μ	s^{-1}	10^{-3}	(17, 18)
λ	nm	5	Table S1
L_{thr}	pM	10	(15)
L_{lo}	pM	10^{-7}	
R_0	$\mu\mathrm{m}^{-2}$	1	(2)

IFN binding affinities (15). The upper bound for the unbinding rates is given by the diffusion-limited binding rate $k_b \leq k_+ = 4\pi Ds$, where D is the sum of the ligand and receptor diffusivities and s is the encounter radius (19). Using typical upper bounds for $D = 10^3 \mu\text{m}^2/\text{s}$ and $s = 10\text{nm}$, one arrives at $k_u = k_+ K^B = 0.06 K^B/(\text{pM s})$ (16). An upper bound for the in-membrane dissociation rate k_d can also be estimated by considering a diffusion-limited association rate k_a. Due to the two-dimensional nature of membrane binding, diffusion-limited rates are not universal, but concentration dependent. We therefore impose a bulk membrane receptor concentration by fixing the mean free distance $2b$ of receptors in the membrane. Then k_a is diffusion-limited by $k_a \leq k_+ = 2\pi D/\ln(b/s)$ (16). Here, D is the sum of free and ligand-bound receptor diffusivities and s is the encounter radius. Using typical values $D = 0.1\mu\text{m}^2/\text{s}$, $s = 10\text{nm}$ and $b = 100\text{nm}$ (16), we obtain $k_d = k_+ K^X \approx 0.3 K^X \frac{\mu\text{m}^2}{s} = 2 \times 10^{-6} \lambda K^B/(\text{nm pM s})$. The maximal lifetimes of both receptor complexes are constrained to ensure numerical stability such that $k_{u,d} \geq 10^{-9}\text{s}^{-1}$.

The remaining parameters $L_{\text{thr}}, L_{\text{lo}}, R_0, \lambda, \mu$ are held at fixed values during optimization, as follows. The detection threshold $L_{\text{thr}} = 10\text{pM}$ is within the range of measured detection thresholds for IFNs (15). As minimum concentration we choose $L_{\text{lo}} = 10^{-7}\text{pM}$, which prevents generating optimal solutions with inverted responses (receptors are only activated at $L < L_{\text{thr}}$) or responses where one ligand activates receptor at any $L \gtrsim L_{\text{thr}}$. For the dimerizing receptor system, we additionally impose a fixed receptor density $R_0 = 1\mu\text{m}^{-2}$ (2) and make the assumption of an unchanged binding mode, implying $\lambda = K^X/K^B$ is a ligand-independent constant given by $\lambda = 5\text{nm}$, see Sec. 3. In receptor systems with turnover, we impose a fixed turnover rate $\mu = 10^{-3}\text{s}^{-1}$ within the measured range for cytokine receptors (17, 18).

The optimal resulting dissociation constants and/or kinetic rates are given in Table S5. In cases where

Table S5. Dissociation constants and unbinding rates for activation curves shown in Figs. 3 and 5

figure	receptor architecture	case	unit	dissociation constants and unbinding rates	unit	peak activation
Fig. 3C	allosteric	I	pM	$K_\alpha = 3300, K_\beta = 1.6$	1	$f_{\text{max},\alpha} = f_{\text{max},\beta} = 1.00$
		II	pM	$K_\alpha = K_\beta = 28$	1	$f_{\text{max},\alpha} = f_{\text{max},\beta} = 1.00$
		III	pM	$K_\alpha = K_\beta = 21$	1	$f_{\text{max},\alpha} = f_{\text{max},\beta} = 1.00$
Fig. 3E	homodimer	I	pM	$K_\alpha^B = 2.0 \times 10^4, K_\beta^B = 960$	1	$f_{\text{max},\alpha} = 0.71, f_{\text{max},\beta} = 0.93$
		IV	pM	$K_\alpha^B = K_\beta^B = 1.0 \times 10^4$	1	$f_{\text{max},\alpha} = f_{\text{max},\beta} = 0.78$
Fig. 3G	heterodimer	I	pM	$K_{\alpha,1}^B = 9.6 \times 10^5, K_{\alpha,2}^B = 4.2$	1	$f_{\text{max},\alpha} = 0.21$
				$K_{\beta,1}^B = 3300, K_{\beta,2}^B = 1700$	1	$f_{\text{max},\beta} = 0.84$
		IV	pM	$K_{\alpha,1}^B = 1.0 \times 10^6, K_{\alpha,2}^B = 33$	1	$f_{\text{max},\alpha} = 0.21$
				$K_{\beta,1}^B = 3900, K_{\beta,2}^B = 3500$	1	$f_{\text{max},\beta} = 0.81$
Fig. 5A	homodimer with turnover	IV	pM	$K_\alpha^B = 1.2 \times 10^4, K_\beta^B = 83$	1	$f_{\text{max},\alpha} = 0.76, f_{\text{max},\beta} = 0.94$
			s^{-1}	$k_{u,a} = 340, k_{u,b} = 1.5 \times 10^{-4}$		
				$k_{d,a} = 0.012, k_{d,b} = 8.3 \times 10^{-5}$		
Fig. 5A	heterodimer with turnover	IV	pM	$K_{\alpha,1}^B = 1.6 \times 10^4, K_{\alpha,2}^B = 27$	1	$f_{\text{max},\alpha} = 0.27$
				$K_{\beta,1}^B = 420, K_{\beta,2}^B = 20$	1	$f_{\text{max},\beta} = 0.93$
			s^{-1}	$k_{u,a,1} = 1.0 \times 10^{-6}, k_{u,a,2} = 0.074$		
				$k_{u,b,1} = 1.0 \times 10^{-6}, k_{u,b,2} = 0.0014$		
				$k_{d,a,1} = 2.6 \times 10^{-5}, k_{d,a,2} = 2.7 \times 10^{-5}$		
				$k_{d,b,1} = 4.2 \times 10^{-4}, k_{d,b,2} = 1.0 \times 10^{-6}$		

figure	receptor architecture	unit	receptor density	unit	ligand range
Fig. 5A	IFN	μm^{-2}	$R_0 = 20$	1	$L_{\text{hi}}/L_{\text{thr}} = 1.2 \times 10^5$

pure presence sensing is optimal, ligands α and β obtain identical kinetic constants. When type sensing is admitted, the stronger ligand β is (by our convention) the ligand with higher peak activation. Notice that heterodimers without turnover can yield optimal dissociation constants where the weaker ligand α shows an earlier activation onset, that is, $K^B_{\alpha,2} < K^B_{\beta,2}$, for instance, in Fig. 3G. This feature is a result of the need for a broad low-activation plateau for the weaker ligand. In systems with turnover, we always observe $K^B_{\alpha,2} > K^B_{\beta,2}$. This ranking is in accordance with literature values for IFNα2 and IFNβ affinities, although measured IFNAR2 affinities differ more strongly. For the IFN activation curve in Fig. 5A, bottom in the main text, we optimized the discrimination power with respect to the receptor density R_0 and the upper cutoff L_{hi}, see Table S5, bottom. As optimization range we used $R_0 = 0.1 - 10^3 \mu\mathrm{m}^{-2}$ and $L_{\mathrm{hi}}/L_{\mathrm{thr}} = 10^2 - 10^6$.

The literature values (extracted and converted from (7, 9, 20, 21)) of the kinetic rates used for the IFN activation curve are summarized in Table S6.

Table S6. Parameter set for IFNα2 and IFNβ

kinetic rate	unit	IFNα2	IFNβ
$k_{b,1}$	$(\mathrm{Ms})^{-1}$	6.7×10^5	5.0×10^5
$k_{u,1}$	s^{-1}	1.0	1.0×10^{-2}
K_1^B	nM	1500	20
$k_{b,2}$	$(\mathrm{Ms})^{-1}$	2.2×10^6	1.0×10^7
$k_{u,2}$	s^{-1}	2.0×10^{-2}	1.0×10^{-3}
K_2^B	pM	9100	100
$k_{a,1}$	$\mu\mathrm{m}^2\mathrm{s}^{-1}$	5.48×10^{-2}	1.67×10^{-2}
$k_{d,1}$	s^{-1}	0.40	3.3×10^{-3}
$k_{a,2}$	$\mu\mathrm{m}^2\mathrm{s}^{-1}$	1.67×10^{-2}	1.67×10^{-2}
$k_{d,2}$	s^{-1}	4.4×10^{-3}	3.3×10^{-4}

6. Molecular noise in receptor activation and cell-to-cell variability in receptor number can be approximated by adjusting the readout number

All readout distributions shown in the main text (cf. Figs. 3-5 and Fig. S4) correspond to a noise model (Eq. (5), main) that includes stochastic activation of readout molecules as the only noise source. In the following we investigate the effect of additional noise sources, namely cell-to-cell variability of receptor numbers and molecular noise in receptor activation.

A. Cell-to-cell variability in receptor number. Cell populations show heterogeneity in protein composition, including bimodal and long-tailed protein number distributions. Here we consider only constitutive genes with unimodal protein number distribution, so that the cell-to-cell variability in receptor numbers can be approximated well by a Gamma distribution $p(r) = \beta^\alpha x^{\alpha-1} e^{-\beta r}/\Gamma(\alpha)$, where r denotes the total number of receptors (22). To include this noise source, we generalize Eq. (5) (main) by introducing an additional sum over the total receptor number. The input-output relation $p(n|x)$ (Eq. (4), main) then becomes

$$p(n|x) = \int \Big[\sum_r p\Big(n|\tfrac{r}{r_{\mathrm{tot}}} f_x(L)\Big) p(r)\Big] p(L|x) dL, \qquad [68]$$

where r_{tot} is the mean total receptor number. Note that in Eq. (4) (main), the total receptor density R_0 was fixed, resulting in a rate of phosphorylation of readout molecules proportional to the activated receptor fraction f. When considering cell-to-cell variability in receptor number, this assumption is not valid anymore and correspondingly, the phosphorylation rate is proportional to the number rf of activated receptors in Eq. (68).

We first investigate how the discrimination power of allosteric receptors is affected by cell-to-cell variability. As a baseline, we compute the optimal activation curves and corresponding readout distributions as in the main text, considering only the readout noise for $\bar{n} = 100$ and $L_{\mathrm{hi}} = 18$nM, Fig. S3A. This corresponds to cases I and III in the main text but with intermediate readout number. We then recalculate the readout distribution using the unchanged activation curves of Fig. S3A, but this time including cell-to-cell variability in receptor number, Eq. (68). We assume an average of $r_{\mathrm{tot}} = 100$ receptors and a coefficient of variation of 25% for the receptor number (23), corresponding to parameters $\alpha = 16$ and $\beta = 0.16$ for $p(r)$. As expected, adding the additional noise term broadens the readout distribution, Fig. S3B, top. Remarkably, comparable broadening and nearly identical distribution shape can be obtained by reducing the readout number $\bar{n}$ from 100 to 20, Fig. S3B bottom.

Next, we repeat this procedure for homodimerizing receptors. As Fig. S3CD show, the results confirm the finding that the cell-to-cell variability can approximated well by reducing the readout number $\bar{n}$ to 20. We remark that, for dimerizing receptors, the activated receptor fraction depends on the receptor density R_0. Therefore, Eq. (68), strictly speaking, represents cells of varying size and total protein number but constant receptor density.

B. Molecular noise in receptor activation. Next, we consider molecular noise in receptor activation as additional noise source. In order to generalize the noise model (Eq. (5), main) we introduce an additional sum over the number of activated receptors a. The input-output relation (Eq. (4), main) becomes

$$p(n|x) = \int \Big[\sum_{a=0}^{r_{\mathrm{tot}}} p\Big(n|\tfrac{a}{r_{\mathrm{tot}}}\Big) p(a|f_x(L), r_{\mathrm{tot}})\Big] p(L|x) dL, \qquad [69]$$

where $p(a|f, r_{\mathrm{tot}})$ is the probability that a out of r_{tot} receptors are activated for a mean activation of $f r_{\mathrm{tot}}$ receptors, which depends on the receptor architecture.

For allosteric receptors, the master equation corresponding to the reaction scheme Eq. (29) results in the binomial distribution

$$p(a|f, r_{\mathrm{tot}}) = \binom{r_{\mathrm{tot}}}{a} f^a (1-f)^{r_{\mathrm{tot}}-a}. \qquad [70]$$

To demonstrate the effect of receptor activation noise, we again start with optimal activation curves for readout noise only, Fig. S3E, and add activation noise by setting $r_{\mathrm{tot}} = \bar{n} = 100$ in Eqs. (69,70). We find only a modest effect on the readout distribution, see Fig. S3EF. Increasing the receptor number to the typical numbers of IFN receptors of a few hundred copies per cell (2) further decreases the effect. Overall, the effect of receptor activation noise is negligible next to typical amounts of cell-to-cell variability (cf. Fig. S3B).

C. Optimal responses including readout noise, activation noise and cell-to-cell variability. We now include both additional noise sources. As in the main text, we optimize the ligand discrimination power I for allosteric receptors over the affinities $K_{\alpha,\beta}$, at $\bar{n} = r_{\mathrm{tot}} = 100$ and $L_{\mathrm{hi}} = 18\mathrm{nM}$, cf. Fig. 3CD. We find that including the additional noise moves the system to the regime of pure presence sensing, *i.e.* discrimination power is optimized by coinciding activation curves with $K_\alpha = K_\beta$, Fig. S3G, top. Nevertheless, a very similar optimization result is obtained by including only readout noise but with reduced readout number $\bar{n} = 20$, Fig. S3G, bottom. We conclude that pure readout noise provides a convenient effective description for the relevant noise sources in ligand discrimination and is sufficient at the level of detail of the present study.

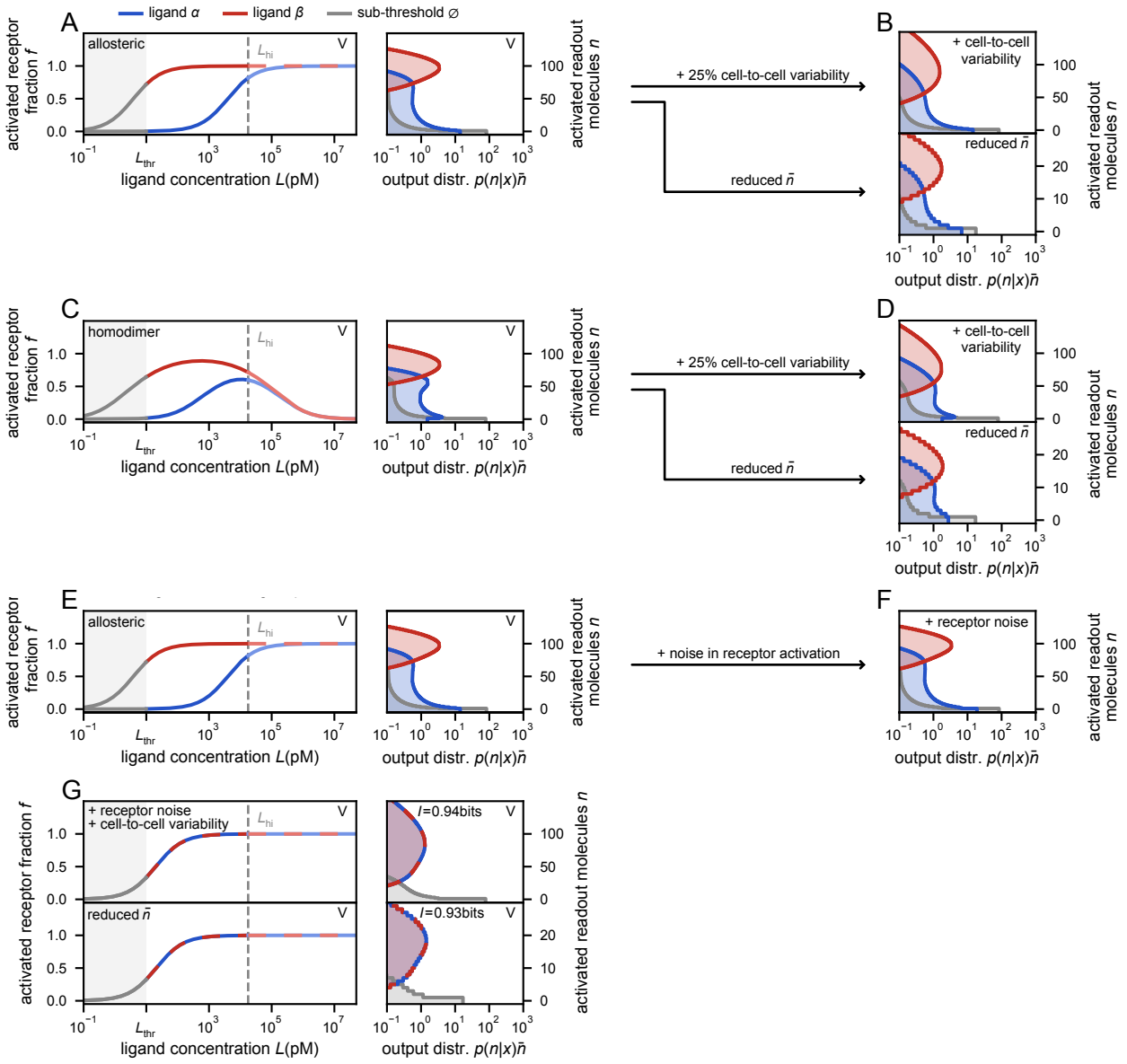

Fig. S3. Effect of additional noise sources in form of cell-to-cell variability in receptor numbers and molecular noise in receptor activation on the readout distribution. (A) Optimal activation curves and corresponding readout distributions for allosteric receptors without additional noise source. Case V (like case I and III in main but with intermediate readout number $\bar{n} = 100$), $K_\alpha = 4.0\mathrm{nM}$, $K_\beta = 3.9\mathrm{pM}$. (B) Readout distribution corresponding to A. Top, including 25% cell-to-cell variability in receptor numbers broadens the readout distributions. Bottom, reducing the readout number to $\bar{n} = 20$ reproduces a similar effect on the readout distributions. (C) Optimal activation curves and corresponding readout distributions for homodimerizing receptors. Case V, $K_\alpha = 21\mathrm{nM}$, $K_\beta = 1.1\mathrm{nM}$. (D) Readout distribution corresponding to C. Effect of including 25% cell-to-cell variability in receptor numbers on the readout distributions (top) can be approximated well by reducing the readout number to $\bar{n} = 20$ (bottom). (E) same as A. (F) Readout distributions for allosteric receptors including molecular noise in receptor activation corresponding to E. (G) Optimal activation curves and corresponding readout distributions for allosteric receptors considering receptor activation noise and 25% cell-to-cell variability (top, $K_\alpha = K_\beta = 20\mathrm{pM}$) almost coincide with optimal solutions for reduced readout number $\bar{n} = 20$ (bottom, $K_\alpha = K_\beta = 21\mathrm{pM}$). Both results in superimposed ligands α and β (dashed curves) with good separation from $\varnothing$, indicating pure presence sensing. Here we used $r_{\mathrm{tot}} = 100$.

7. Optimal responses for alternative input distributions

The discrimination power I depends on the chosen input distribution $p(x)$, see Eq. (1) in the main text. Throughout the main text we chose $p(\varnothing) = 2p(\alpha) = 2p(\beta) = 1/2$, which represents equal probabilities for ligand presence and absence, and for either ligand if present. To explore how the optimal power and ligand discrimination strategy of receptor systems change with the input distribution, in this subsection we re-optimize ligand discrimination power with two plausible alternative choices for $p(x)$, corresponding to rare inflammation and unequal ligand abundances, respectively. The results can be rationalized by considering the general upper bound for mutual information involving a binary variable (presence or type) with values $i = 1, 2$,

$$I \leq H[p(i)] = -p(1)\log_2 p(1) - p(2)\log_2 p(2). \qquad [71]$$

A. Rare inflammation. When inflammation is a rare occurrence, the probability of ligand being present decreases, $p_\pi = 1 - p(\varnothing) < 1/2$. The upper bound Eq. (71) for presence information I_π decreases for smaller p_π. The upper bound for type information I_τ is unaffected, but I_τ occurs with a reduced prefactor in $I = I_\pi + p_\pi I_\tau$; we consider the exemplary cases $p_\pi = 0.25$, where $I \leq 1.06$ bits and $p_\pi = 0.1$, where $I \leq 0.57$ bits. Overall the contribution from type sensing is reduced more strongly, so that lower p_π puts more importance on achieving good presence sensing compared to type sensing. As a result, the regime where pure presence sensing is preferred extends to higher readout numbers and/or lower concentration ranges for allosteric and homodimerizing receptor architectures, compare Figs. S4A1,A2 and S4D1,D2 ($p_\pi = 0.25$). For even lower ligand prevalence ($p_\pi = 0.1$) the regime extends over the full parameter range tested, Fig. S4E-G,1-2. By contrast, the heterodimerizing system can reconcile presence and type sensing also for lower p_π, as activation curves can exploit distinct activation plateaus Fig. S4D3-G3. Note however that also in the heterodimerizing system, the overlap between output distributions for α and β ligands is increased due to the lower importance of type sensing, see Fig. S4B3,C3,F3,G3.

B. Unequal ligand abundance. We now consider a scenario where the weaker ligand α occurs more frequently than the stronger ligand β, which is plausible when a more drastic inflammatory response is required only in the most extreme circumstances. We keep $p_\pi = 1/2$ for simplicity. When $p_\tau(\beta) < 0.5$, the upper bound Eq. (71) for type information decreases; the upper bound for presence information is unchanged. Thus, also in the unequal ligands scenario, more importance is placed on achieving good presence sensing compared to type sensing. Overall, the discrimination power $I \leq 1.41$ bits for $p_\tau(\beta) = 0.25$ and $I \leq 1.23$ bits for $p_\tau(\beta) = 0.1$. As expected by these considerations, the optimization of discrimination power with unequal ligand abundances yields similar results as in the case of rare inflammation. For allosteric and homodimerizing receptors, the region of pure presence sensing increases towards higher readout numbers and/or narrower concentration ranges, compare Figs. S4A1,A2 and S4H1,H2 ($p_\tau(\beta) = 0.25$), and eventually covers the full parameter range, Fig. S4I-K,1-2 ($p_\tau(\beta) = 0.1$). As before, the heterodimerizing system can reconcile presence and type sensing Fig. S4H3-K3.

Overall, considering rare inflammation or unequal ligand abundance cause presence sensing to be preferred over a wider range. Heterodimerizing receptors continue to accommodate type sensing and remain superior to the allosteric and homodimerizing receptors. Within each regime, the optimal activation curves are

virtually unchanged by the changes in input distribution (Fig. S4BCFGJK, cf. Fig. 3CEG). Thus the main effect of the input distribution is a redistribution of importance between presence and type sensing, which does not affect the performance ranking of different receptor architectures.

The optimal resulting dissociation constants and/or kinetic rates are given in Table S7.

Table S7. Dissociation constants for activation curves shown in Fig. S4

figure	receptor architecture	dissociation constants (pM)	peak activation
B1	allosteric	$K_\alpha = 4000$, $K_\beta = 3.9$	$f_{\mathrm{max},\alpha} = f_{\mathrm{max},\beta} = 1.00$
B2	homodimer	$K_\alpha^B = 3.0 \times 10^4$, $K_\beta^B = 1400$	$f_{\mathrm{max},\alpha} = 0.65$, $f_{\mathrm{max},\beta} = 0.91$
B3	heterodimer	$K_{\alpha,1}^B = 8.1 \times 10^5$, $K_{\alpha,2}^B = 11$	$f_{\mathrm{max},\alpha} = 0.24$
		$K_{\beta,1}^B = 1600$, $K_{\beta,2}^B = 1400$	$f_{\mathrm{max},\beta} = 0.87$
F1	allosteric	$K_\alpha = K_\beta = 22$	$f_{\mathrm{max},\alpha} = f_{\mathrm{max},\beta} = 1.00$
F2	homodimer	$K_\alpha^B = K_\beta^B = 6000$	$f_{\mathrm{max},\alpha} = f_{\mathrm{max},\beta} = 0.83$
F3	heterodimer	$K_{\alpha,1}^B = 4.5 \times 10^5$, $K_{\alpha,2}^B = 22$	$f_{\mathrm{max},\alpha} = 0.33$
		$K_{\beta,1}^B = 8700$, $K_{\beta,2}^B = 1500$	$f_{\mathrm{max},\beta} = 0.81$
J1	allosteric	$K_\alpha = K_\beta = 17$	$f_{\mathrm{max},\alpha} = f_{\mathrm{max},\beta} = 1.00$
J2	homodimer	$K_\alpha^B = K_\beta^B = 5000$	$f_{\mathrm{max},\alpha} = f_{\mathrm{max},\beta} = 0.84$
J3	heterodimer	$K_{\alpha,1}^B = 1.1 \times 10^6$, $K_{\alpha,2}^B = 12$	$f_{\mathrm{max},\alpha} = 0.20$
		$K_{\beta,1}^B = 2100$, $K_{\beta,2}^B = 1600$	$f_{\mathrm{max},\beta} = 0.86$

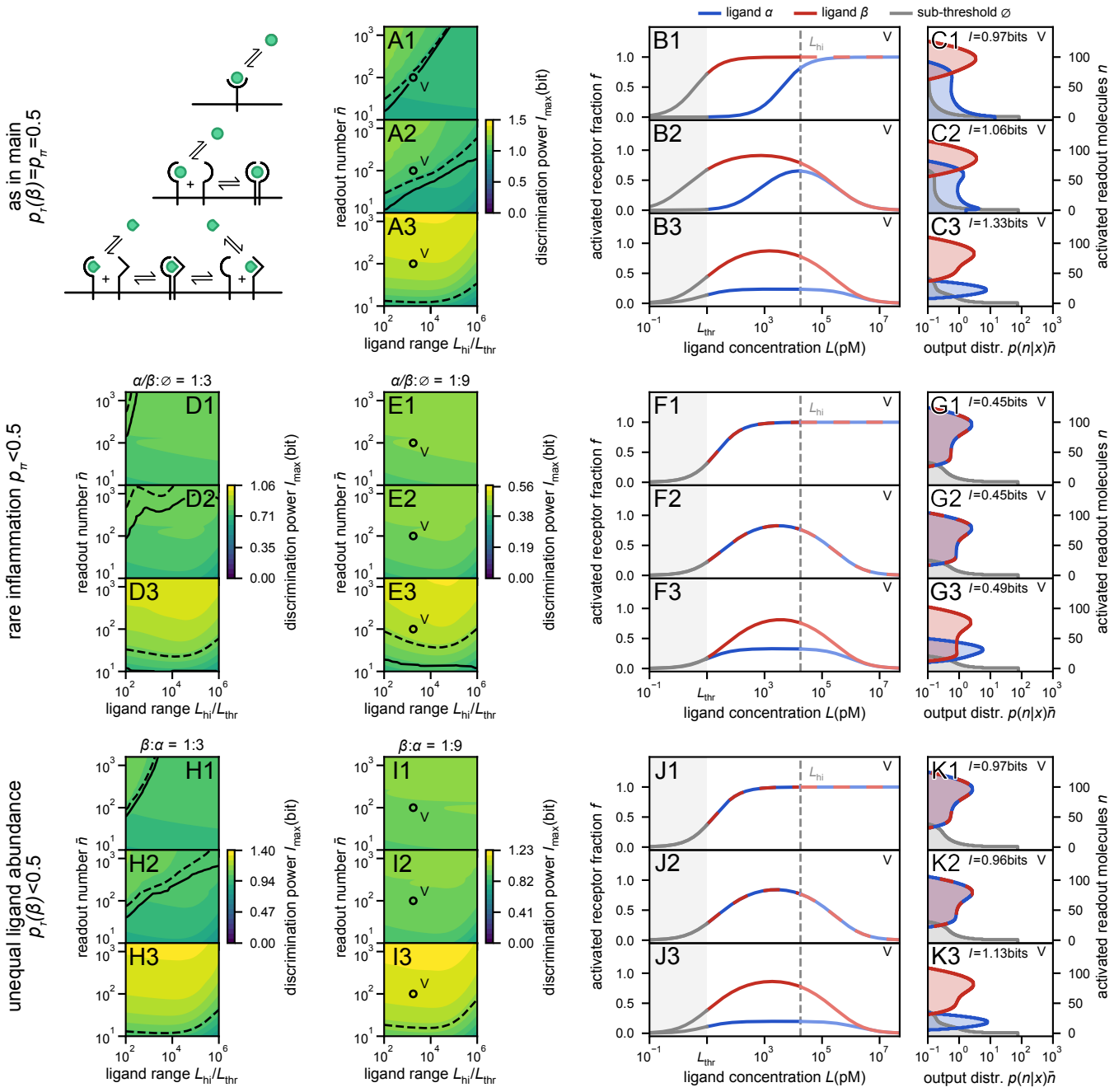

Fig. S4. Ligand discrimination in allosteric (1), homodimerizing (2) and heterodimerizing (3) receptors for different input distributions. (A) Optimal discrimination power *vs.* concentration range and readout number as in Fig. 4B-D. (B) Optimal activation curves for case V. Ligands are separated for all basic receptors. (C) Readout distributions corresponding to B. Receptor 1 and 2, α and β are separated but α overlaps with ∅. 3, α, β and ∅ are well separated. (DE) Optimal discrimination power *vs.* concentration range and readout number for rare inflammation: $p_\pi = 0.25$ (D) and $p_\pi = 0.1$ (E). (F) Optimal activation curves for rare inflammation. Equal affinities for ligands are optimal in receptor 1 and 2, but ligands are separated in 3. (G) Readout distributions corresponding to F. Receptor 1 and 2, pure presence sensing. 3, α, β and ∅ are well separated. (HI) Optimal discrimination power *vs.* concentration range and readout number for unequal ligand abundance: $p_r(\beta) = 0.25$ (H) and $p_r(\beta) = 0.1$ (I). (J) Optimal activation curves for rare inflammation. Equal affinities for ligands are optimal in receptor 1 and 2, but ligands are separated in 3. (K) Readout distributions corresponding to F. Receptor 1 and 2, pure presence sensing. 3, α, β and ∅ are well separated. Optimal parameter values are detailed in Supplementary Table S7.

References

1. C Gardiner, *Stochastic methods.* (Springer Berlin) Vol. 4, (2009).
2. J Piehler, C Thomas, KC Garcia, G Schreiber, Structural and dynamic determinants of type I interferon receptor assembly and their functional interpretation. *Immunol. reviews* **250**, 317–34 (2012).
3. G Altan-Bonnet, T Mora, AM Walczak, Quantitative immunology for physicists. *Phys. Reports* **849**, 1–83 (2020).
4. ET Jaynes, GL Bretthorst, *Probability Theory: The Logic of Science.* (Cambridge University Press, Cambridge, UK), (2003).
5. A Oyler-Yaniv, et al., A Tunable Diffusion-Consumption Mechanism of Cytokine Propagation Enables Plasticity in Cell-to-Cell Communication in the Immune System. *Immunity* **46**, 609–620 (2017).
6. S Fathi, CR Nayak, JJ Feld, AG Zilman, Absolute Ligand Discrimination by Dimeric Signaling Receptors. *Biophys. J.* **111**, 917–920 (2016).
7. F Roder, S Wilmes, CP Richter, J Piehler, Rapid Transfer of Transmembrane Proteins for Single Molecule Dimerization Assays in Polymer-Supported Membranes. *ACS Chem. Biol.* **9**, 2479–2484 (2014).
8. M Gavutis, S Lata, P Lamken, P Müller, J Piehler, Lateral ligand-receptor interactions on membranes probed by simultaneous fluorescence-interference detection. *Biophys. journal* **88**, 4289–302 (2005).
9. M Gavutis, E Jaks, P Lamken, J Piehler, Determination of the two-dimensional interaction rate constants of a cytokine receptor complex. *Biophys. journal* **90**, 3345–55 (2006).
10. S Wilmes, et al., Receptor dimerization dynamics as a regulatory valve for plasticity of type I interferon signaling. *The J. Cell Biol.* **209**, 579–593 (2015).
11. AS Perelson, G Weisbuch, Immunology for physicists. *Rev. Mod. Phys.* **69**, 1219–1268 (1997).
12. AS Perelson, Receptor clustering on a cell surface. II. theory of receptor cross-linking by ligands bearing two chemically distinct functional groups. *Math. Biosci.* **49**, 87–110 (1980).
13. Y Xiang, DY Sun, W Fan, XG Gong, Generalized simulated annealing algorithm and its application to the Thomson model. *Phys. Lett. A* **233**, 216 – 220 (1997).
14. P Virtanen, et al., SciPy 1.0: Fundamental Algorithms for Scientific Computing in Python. *Nat. Methods* **17**, 261–272 (2020).
15. TB Lavoie, et al., Binding and activity of all human alpha interferon subtypes. *Cytokine* **56**, 282–289 (2011).
16. DA Lauffenburger, JJ Linderman, *Receptors : models for binding, trafficking, and signaling.* (Oxford University Press, New York), (1993).
17. KGS Kumar, et al., Site-specific ubiquitination exposes a linear motif to promote interferon-alpha receptor endocytosis. *J. Cell Biol.* **179**, 935–950 (2007) Publisher: The Rockefeller University Press.
18. KGS Kumar, et al., Basal Ubiquitin-independent Internalization of Interferon alpha Receptor Is Prevented by Tyk2-mediated Masking of a Linear Endocytic Motif. *The J. Biol. Chem.* **283**, 18566–18572 (2008).
19. D Shoup, A Szabo, Role of diffusion in ligand binding to macromolecules and cell-bound receptors. *Biophys. J.* **40**, 33–39 (1982).

20. C You, et al., Receptor dimer stabilization by hierarchical plasma membrane microcompartments regulates cytokine signaling. *Sci. Adv.* **2**, 1–13 (2016).
21. E Jaks, M Gavutis, G Uzé, J Martal, J Piehler, Differential receptor subunit affinities of type I interferons govern differential signal activation. *J. molecular biology* **366**, 525–39 (2007).
22. N Friedman, L Cai, XS Xie, Linking Stochastic Dynamics to Population Distribution: An Analytical Framework of Gene Expression. *Phys. Rev. Lett.* **97**, 168302 (2006).
23. A Bar-Even, et al., Noise in protein expression scales with natural protein abundance. *Nat. Genet.* **38**, 636–643 (2006).